Int. J. Heat Mass Transfer. Vol. 24, No. 4, pp. 659–669, 1981
Printed in Great Britain

0017–9310/81/040659–11 $02.00/0

TURBULENT MHD FLOW OF A RADIATING GAS

THEODORE F. SMITH, FARIBORZ ALIPOUR-HAGHIGHI and PHILLIP H. PAUL*
Division of Energy Engineering, The University of Iowa,
Iowa City, IA 52242, U.S.A.

(*Received* 13 *November* 1979 *and in revised form* 24 *September* 1980)

Abstract— The high temperatures and gaseous products of combustion of hydrocarbon fuels in proposed large scale magnetohydrodynamic generators have resulted in a need to develop accurate models for prediction of gas temperature profiles and wall heat fluxes. At the high temperatures and large sizes, radiative heat transfer in the combustion gases may be a significant energy transport mechanism. Results are presented for gas temperature profiles for fully developed turbulent magnetohydrodynamic flow of a radiating gray gas between infinite parallel plates with a magnetic field applied perpendicular to the plates. Emphasis is placed on examination of temperature profiles and Nusselt numbers for various values of Hartmann and Reynolds numbers, gas optical thickness, and conduction to radiation parameter.

NOMENCLATURE

A_i, coefficients defined by equation (28);
$\bar{A}$, van Driest constant, 26.0;
$\bar{b}$, Mei and Squire constant, 3.4;
B_b, black body emissive power [W/m^2];
B_m, magnetic field [Webers/m^2];
$\bar{B}$, magnetic interaction, Ha^2/Re;
c_p, constant pressure specific heat [kJ/kg-K];
C_f, friction coefficient;
C_i, terms defined by equation (29);
D, magnetic damping function;
D_e, hydraulic diameter [m];
D_i, terms defined by equation (30);
E, electric field [V/m];
Ec, Eckert number, $\bar{v}^2/c_pT_w$;
E_n, exponential integral of order n;
F_1, function defined by equation (7);
Ha, Hartmann number, $\delta B_m(\sigma_e/\mu)^{1/2}$;
j, current density [A/m^2];
J, dimensionless current, $j/\sigma_e\bar{v}B_m$;
k, thermal conductivity [W/m-K];
K, power factor, $E/\bar{v}B_m$;
K_1, K_2, kernels defined by equations (16) and (20);
$\bar{K}$, Von Karman constant, 0.4;
L, channel width [m];
M, number of nodal points;
N, conduction to radiation parameter, $k\kappa/4\sigma T_w^3$;
Nu, Nusselt number, $D_eq_w/k(T_w - T_b)$;
Pr, Pr_t, molecular and turbulent Prandtl numbers, ν/α, ν_t/α_t;
q, heat flux [W/m^2];
Q, dimensionless heat flux, $-q/4\tau_0\sigma T_w^4$;
Re, channel Reynolds number, $v_c\delta/\nu$;
Re_D, hydraulic Reynolds number, v_cD_e/ν;
Re_t, turbulent Reynolds number, $Re(C_f/2)^{1/2}$;
t, parameter;
T, temperature [K];
v, velocity [m/s];
$v_c, \bar{v}$, centerline and mean velocities [m/s];
V, normalized velocity, $v/\bar{v}$;
V_t, scaling factor, $4\,Re_t$;
x, y, z, coordinates [m];
$\bar{z}$, turbulent coordinate.

Greek symbols

α, α_t, molecular and turbulent diffusivities [m^2/s];
δ, channel half width [m];
ζ, parameter;
η, dimensionless coordinate, z/δ;
θ, normalized temperature, T/T_w;
κ, absorption coefficient [m^{-1}];
μ, dynamic viscosity [kg/m-s];
ν, ν_t, molecular and turbulent viscosities [m^2/s];
ξ, logarithmic coordinate defined in equation (31);
σ, Stefan–Boltzmann constant [W/m^2-K^4];
σ_e, electrical conductivity [Ω^{-1} m^{-1}];
τ, optical thickness, κz;
τ_0, channel optical thickness, κL.

Subscripts

b, bulk;
c, convective;
r, radiative;
w, wall.

INTRODUCTION

THE HIGH temperatures of gaseous products resulting from combustion of hydrocarbon fuels have resulted in a need to develop more accurate models for prediction of gas temperature profiles and wall heat fluxes in the magnetohydrodynamic generator (MHD). Information concerned with gas temperature profiles parti-

* Presently, Research Assistant, Stanford University.

cularly near the generator walls is necessary in order to evaluate the gas electrical conductivity and associated wall heat fluxes. Successful design of a wall cooling system and selection of materials for the generator walls also require estimates for wall heat fluxes. At the high operating temperatures and in the presence of combustion products of carbon dioxide and water vapor, particles, as well as a seed material which acts as a plasma, radiative heat transfer is expected to become an important factor as the size of the generator increases [1]. The overall objective of this research is an examination of radiative transfer in MHD flows. Results from this study are also expected to find application to gas-cooled nuclear reactors and flow of plasma.

Viskanta [2,3], Cramer and Pai [4] as well as Wilson and Haji-Sheikh [5] examined radiative transfer for MHD flow between infinite parallel plates for gray gas properties where the absorption coefficient is independent of frequency. Gupta and Gupta [6] as well as Datta and Janta [7] investigated radiative transfer effects for flow of an optically thin, electrically conducting fluid in a vertical channel. Helliwell [8,9] as well as Helliwell and Mosa [10] utilized the differential approximation [11] to describe radiative transfer in MHD channel flow. Smith and Paul [12] employed a band absorption model to examine radiative transfer in MHD flow. In these investigations, the flow was assumed laminar with several of the analyses [2, 3, 5, 8–10, 12] utilizing velocity profiles as obtained from the Hartmann MHD flow results [13]. In most MHD generators, however, the flow is expected to be turbulent and results derived from these analyses may not be directly applicable to proposed generators. This concern is illustrated by the fact that a Hartmann number of 200 which is representative of that for the U-25 channel [14] yields physically unreasonably high channel centerline temperatures when inserted into the above analyses. Consequently, a need exists to provide results concerned with radiative transfer in turbulent MHD flows.

The purpose of this paper is to present results to illustrate effects of radiative transfer in turbulent MHD flow. The system selected for study as depicted in Fig. 1 consists of hydrodynamically and thermally established turbulent steady flow of an electrically conducting and radiatively participating gas between two infinite parallel plates with an imposed uniform and constant magnetic field applied in the positive z-direction. A constant electric field is applied in the positive y-direction. This system was chosen for convenience of including MHD effects and enabling the radiative transfer contribution to be evaluated. Analyses and results presented here, however, are expected to be applicable to more comprehensive MHD flow models. Channel walls are isothermal and black for radiative transfer purposes. Physical properties of the gas are constant. The gas is in local thermodynamic equilibrium and emits and absorbs thermal radiation with a constant absorption coefficient. The gas has a refractive index of unity, and scattering effects are negligible. Results are sought for gas temperature profiles and Nusselt numbers as functions of system parameters.

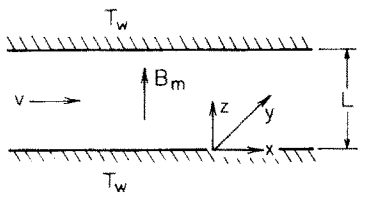

FIG. 1. Schematic diagram of MHD channel.

ANALYSIS

Energy balance

The thermal energy equation for fully developed turbulent flow of an electrically conducting and radiatively participating gas between infinite parallel plates where viscous dissipation and Joule heating effects are considered but axial components of conductive, convective and radiative transfer are neglected is [13, 15, 16]

$$\frac{\mathrm{d}}{\mathrm{d}z}\left[k\left(1+\frac{\alpha_t}{\alpha}\right)\frac{\mathrm{d}T}{\mathrm{d}z}\right] = -\mu\left(1+\frac{\nu_t}{\nu}\right)\left(\frac{\mathrm{d}v}{\mathrm{d}z}\right)^2 - \frac{j^2}{\sigma_e} + \frac{\mathrm{d}q_r}{\mathrm{d}z} \quad (1)$$

where constant properties have been assumed throughout. In equation (1), the LHS represents the net thermal energy transport due to molecular conduction and turbulent transport with α_t denoting the turbulent diffusivity of heat. The terms on the RHS are in the order shown the molecular and turbulent viscous dissipation with ν_t being the turbulent viscosity of momentum, Joulean heating with σ_e denoting the gas electrical conductivity, and divergence of the radiative flux. Both the turbulent transport quantities are assumed to vary across the channel. The boundary conditions for the temperature distribution are $T(0) = T(L) = T_w$. The following dimensionless quantities are introduced

$$\eta = \frac{z}{\delta}, \quad \theta = \frac{T}{T_w}, \quad V = \frac{v}{\bar{v}},$$

$$Pr = \frac{\nu}{\alpha}, \quad Pr_t = \frac{\nu_t}{\alpha_t}, \quad Ec = \frac{\bar{v}^2}{c_p T_w}$$

$$Ha = \delta B_m\left(\frac{\sigma_e}{\mu}\right)^{1/2}, \quad J = \frac{j}{\sigma_e \bar{v} B_m},$$

$$N = \frac{k\kappa}{4\sigma T_w^3}, \quad \tau_0 = \kappa L, \quad Q = \frac{-q}{4\tau_0 \sigma T_w^4} \quad (2)$$

where Pr and Pr_t denote the molecular and turbulent Prandtl numbers, respectively. Ha is the Hartmann number based on the half-channel width δ, and N represents the ratio of molecular thermal conduction

to radiation for a gas with an absorption coefficient κ and optical thickness τ_0 based on the channel width. Equation (1) thus becomes

$$\frac{\mathrm{d}}{\mathrm{d}\eta}\left[\left(1+\frac{Pr}{Pr_t}\frac{\nu_t}{\nu}\right)\frac{\mathrm{d}\theta}{\mathrm{d}\eta}\right] = -PrEc \times\left[\left(1+\frac{\nu_t}{\nu}\right)\left(\frac{\mathrm{d}V}{\mathrm{d}\eta}\right)^2 + Ha^2J^2\right] - \frac{\tau_0^2}{2N}\frac{\mathrm{d}Q_r}{\mathrm{d}\eta} \quad (3)$$

with boundary conditions $\theta(0) = \theta(2) = 1$. As a result of the numerical scheme employed to solve equation (3), the derivative on the LHS was retained. Since Q_r is expressed by an integral term with temperature appearing to the fourth power in the integrand, equation (3) constitutes a second-order, non-linear, integrodifferential equation for the gas temperature distribution. In order to predict the gas temperature profiles, expressions for gas velocity profiles, turbulent viscosity, current density, and radiative flux must be specified and are provided in the following sections.

Velocity, turbulent viscosity, and current models

The flow in several proposed MHD power generators such as the U-25 is subsonic and turbulent. Thus, in considering subsonic flow, the relation of the turbulent boundary layer and free stream is assumed to be similar to that encountered in ordinary hydrodynamic (OHD) flows where magnetic effects are absent. Kruger and Sonju [17] by employing the Karman–Pohlhausen technique have provided an estimate of wall shear stress and boundary-layer thickness corresponding to the semi-empirical velocity correlations proposed by Harris [18]. The local velocity normalized with the centerline value is evaluated from

$$\frac{v(\eta)}{v_c} = \left(\frac{C_f}{2}\right)^{1/2}\left[6.154 + 2.457 \times \ln(Re_t\eta) + F_1\left(\frac{Ha^2}{Re_t}\eta\right)\right]. \quad (4)$$

Kruger and Sonju [17] noted that for MHD flow over a flat plate, the boundary-layer thickness and wall shear stress approach asymptotic values. Since the present study addresses fully developed flow conditions, the asymptotic value for wall shear stress was employed for the friction coefficient in equation (4). Graphical results for the asymptotic friction coefficient presented by Kruger and Sonju [17] are approximated by

$$\frac{C_f}{2} = [10.536 + 0.929\ln(\bar{B}) + 0.0222\ln^2(\bar{B})] \times 10^{-3} \quad (5)$$

where $\bar{B}(= Ha^2/Re^2)$ is the interaction parameter. The turbulent Reynolds number is defined as

$$Re_t = Re\left(\frac{C_f}{2}\right)^{1/2} = \frac{Re_D}{4}\left(\frac{C_f}{2}\right)^{1/2} \quad (6)$$

where Re $(=Re_D/4)$ and Re_D $(=4v_c\delta/\nu)$ denote the channel and hydraulic Reynolds numbers, respectively. The function $F_1(\zeta)$ is presented graphically by Harris [18] and is approximate by the following expression [17] for $\zeta \leq 0.6$

$$F_1(\zeta) = 2.502 + 21.930\zeta - (6.259 + 53.747\zeta + 649.535\zeta^2)^{1/2} \quad (7a)$$

and for $\zeta > 0.6$

$$F_1(\zeta) = -2.07 - 2.457\ln(\zeta). \quad (7b)$$

Near the wall when η is small, velocities evaluated from equation (4) become negative as a result of the logarithmic term. Therefore, in a manner similar to that employed in OHD turbulent flows for the laminar sublayer, velocities are calculated utilizing the product of $Re_t\eta$ up to the position where this product equals equation (4). The mean velocity is determined by integration of the local velocities across the half-channel width. The velocity ratio V is then formed by dividing the local velocities by the mean velocity. Finally, differentiation of the velocity ratio yields the velocity gradient for insertion into the viscous dissipation term of equation (3).

Expressions for the turbulent viscosity for MHD flow are generally based on those for turbulent viscosity for OHD flow with modifications to account for such factors as the damping of the turbulent viscosity as the magnetic field is increased. For the present study, the OHD turbulent viscosity model of van Driest [19] as modified by the Mei and Squire channel factor [20] is utilized with a multiplicative magnetic damping function utilized by Fiveland [21]. Thus,

$$\frac{\nu_t}{\nu} = \frac{0.5D}{1+\bar{b}\eta}\{[1+4\bar{K}^2\bar{z}^2(1-\mathrm{e}^{-\bar{z}/\bar{A}})^2]^{1/2}-1\} \quad (8)$$

where $\bar{b}$, $\bar{K}$, and $\bar{A}$ are the Mei and Squire, Von Karman, and van Driest constants, respectively, and the turbulent distance is

$$\bar{z} = \eta Re_t. \quad (9)$$

The magnetic damping function is [21]

$$D = \mathrm{e}^{-700\,Ha^2/Re_t^2}. \quad (10)$$

The OHD turbulent viscosity model has also been employed by Edwards and Balakrishnan [22] in studies of turbulent channel flow of a radiating gas. The turbulent Prandtl number is assumed unity for the results presented here.

The electrically conducting gas moving through the imposed magnetic field produces an induced current flowing in the negative y-direction of Fig. 1. In dimensionless form, the induced current is [13, 17]

$$J(\eta) = K - V(\eta) \quad (11)$$

where the power factor $K = E/\bar{v}B_m$ with E representing the applied electric field. If $K = 1$, an open circuit exists and the net current given by the integration of equation (11) across the channel is zero. A short circuit

results in $E = K = 0$. Values of $K < 1$ and > 1 imply, respectively, to an MHD generator and pump. The additional Joulean dissipation due to turbulent fluctuations in the velocity [18] is neglected [21].

Radiative transfer model

The formulation of the gas radiative transfer model considers the gas to have a constant absorption coefficient. From Sparrow and Cess [16], the radiative flux for an emitting and absorbing gray gas in local thermodynamic equilibrium is

$$q_r(\tau) = 2E_b(0)[E_3(\tau) - E_3(\tau_0 - \tau)] + 2\int_0^{\tau_0} E_b(t)E_2(|\tau - t|)\mathrm{sgn}(\tau - t)\mathrm{d}t \quad (12)$$

where optical thickness is defined as $\tau = \kappa z$. E_2 and E_3 denote second and third exponential integrals, respectively. E_b is the black body emissive power given by the Stefan–Boltzmann law. The wall radiative flux is needed in the Nusselt number expressions discussed later and is found by evaluating equation (12) at the wall where $\tau = 0$. Thus, with $E_3(0) = 1/2$

$$q_r(0) = 2E_b(0)\left[\frac{1}{2} - E_3(\tau_0)\right] - 2\int_0^{\tau_0} E_b(t)E_2(t)\mathrm{d}t. \quad (13)$$

Introducing the dimensionless parameters defined by equation (2) and the integral property of the exponential integrals, equation (13) is transformed to

$$Q_r(0) = \frac{1}{4}\int_0^2 (\theta^4 - 1)E_2\left(\frac{\tau_0}{2}\eta\right)\mathrm{d}\eta. \quad (14)$$

Recognizing that the temperature profiles are symmetric about the channel centerline, wall heat flux may be evaluated from

$$Q_r(0) = \frac{1}{4}\int_0^1 (\theta^4 - 1)K_1(\eta)\mathrm{d}\eta \quad (15)$$

where the kernel K_1 is defined as

$$K_1(\eta) = E_2\left(\frac{\tau_0}{2}\eta\right) + E_2\left[\frac{\tau_0}{2}(2 - \eta)\right]. \quad (16)$$

The above form for wall radiative flux is convenient since the numerical integration is carried out only for one-half of the channel.

The divergence of radiative flux needed for solution of equation (3) is found by differentiation of equation (12) with respect to τ. Thus,

$$\frac{\mathrm{d}q_r}{\mathrm{d}\tau} = 4E_b(\tau) - 2E_b(0)[E_2(\tau) + E_2(\tau_0 - \tau)] - 2\int_0^{\tau_0} E_b(t)E_1(|\tau - t|)\mathrm{d}t \quad (17)$$

where E_1 is the first exponential integral. Introducing the technique presented by Mingle [23] for removal of the singularity in the integral of the first exponential integral, and the dimensionless variables, equation (17) becomes

$$\frac{\mathrm{d}Q_r}{\mathrm{d}\eta} = \frac{\tau_0}{8}\int_0^2 [\theta^4(\zeta) - \theta^4(\eta)] \times E_1\left[\frac{\tau_0}{2}(|\eta - \zeta|)\right]\mathrm{d}\zeta - \frac{1}{4}[\theta^4(\eta) - 1]K_1(\eta). \quad (18)$$

Finally, employing the symmetric temperature profile conditions, the divergence of the radiative flux is

$$\frac{\mathrm{d}Q_r}{\mathrm{d}\eta} = \frac{\tau_0}{8}\int_0^1 [\theta^4(\zeta) - \theta^4(\eta)] \times K_2(\eta, \zeta)\mathrm{d}\zeta - \frac{1}{4}[\theta^4(\eta) - 1]K_1(\eta) \quad (19)$$

where the kernel K_2 is defined as

$$K_2(\eta, \zeta) = E_1\left[\frac{\tau_0}{2}(|\eta - \zeta|)\right] + E_1\left[\frac{\tau_0}{2}(2 - \zeta - \eta)\right]. \quad (20)$$

Hence, only information about temperature profiles in the half-channel is needed.

Wall heat flux and Nusselt numbers

The wall heat flux is the sum of the conductive and radiative fluxes evaluated at the wall and is given by

$$q_w = -k\left.\frac{\mathrm{d}T}{\mathrm{d}z}\right|_{z=0} + q_r(0) \quad (21)$$

which may be expressed as

$$Q_w = \frac{N}{\tau_0^2}\left.\frac{\mathrm{d}\theta}{\mathrm{d}\eta}\right|_{\eta=0} + Q_r(0). \quad (22)$$

Another quantity of interest is the Nusselt number defined in terms of the wall heat flux and hydraulic diameter as

$$Nu = \frac{D_e q_w}{k(T_w - T_b)} \quad (23)$$

where T_b is the bulk fluid temperature. Equation (22) in conjunction with equation (23) transform to

$$Nu = Nu_c + Nu_r \quad (24)$$

where convective and radiative Nusselt numbers are defined respectively as

$$Nu_c = \frac{4}{\theta_b - 1}\left.\frac{\mathrm{d}\theta}{\mathrm{d}\eta}\right|_{\eta=0}; \qquad Nu_r = \frac{4\tau_0^2}{(\theta_b - 1)N}Q_r(0). \quad (25)$$

The bulk fluid temperature is found from

$$\theta_b = \int_0^1 \theta V\,\mathrm{d}\eta. \quad (26)$$

The above definition of the convective Nusselt number includes effects attributed to radiative transfer since

the gas temperature gradient at the wall is partially governed by the radiant exchange process.

METHOD OF SOLUTION

Solutions of the energy equation were arrived at by a finite difference scheme where equation (3) was replaced with a set of linear algebraic equations with the source and nonlinear terms on the RHS of equation (3) assumed known. An iterative technique was then utilized since the radiative term varies with temperature. The finite difference scheme for symmetry conditions about the channel centerline yields the following set of algebraic equations for the temperatures

$$A_{i-1}\theta_{i-1} - (A_{i-1} + A_i)\theta_i + A_i\theta_{i+1} = -C_i - D_1; \quad i = 2 \text{ to } M-1 \tag{27a}$$

$$2A_{M-1}(\theta_{M-1} - \theta_M) = -C_M - D_M \tag{27b}$$

where $i = 1$ and M correspond to positions at the channel wall and centerline, respectively, and $\theta_1 = 1.0$. The coefficients of θ_i are evaluated from

$$A_i = \left(1 + \frac{Pr}{Pr_t}\frac{\nu_t}{\nu}\right)_{i+1/2} \Big/ (\eta_{i+1} - \eta_i); \quad i = 1 \text{ to } M-1 \tag{28}$$

where the subscript $i + 1/2$ denotes that the quantity is to be evaluated at the midpoint between adjacent nodes. Also, $\eta_1 = 0$, and $\eta_M = 1.0$. The temperature independent source terms of viscous dissipation and Joulean heating are represented by C_i which are determined from

$$C_i = \Delta\eta_i PrEc\left[\left(1 + \frac{\nu_t}{\nu}\right)\left(\frac{dV}{d\eta}\right)^2 + Ha^2J^2\right]_i; \quad i = 2 \text{ to } M \tag{29}$$

where $\Delta\eta_i$ is the width of each node. Nodal boundaries are placed at the midpoint between adjacent nodes. The temperature dependent radiative terms described by D_i are given as

$$D_i = \Delta\eta_i \frac{\tau_0^2}{2N}\left.\frac{dQ_r}{d\eta}\right|_i; \quad i = 2 \text{ to } M \tag{30}$$

With the source terms known, equation (27) was solved utilizing a tridiagonal matrix algorithm. The iteration scheme consisted of specification of an initial temperature distribution to evaluate the radiative term. New temperatures from equation (27) were then obtained. If the new temperatures upon comparison with the previous temperatures do not satisfy a convergence error criterion, the previous temperatures were adjusted with a relaxation factor multiplied by the difference between the new and previous temperatures and the iteration process repeated. The relaxation factor whose value was typically 0.1 was employed to ensure that nonlinearities attributed to the radiative term were suppressed and that convergence could be obtained. Upon achievement of convergence, the bulk fluid temperature, wall heat fluxes, and Nusselt numbers were calculated. Integrals appearing in the analysis were evaluated utilizing a variable spacing trapezoidal integration algorithm.

For turbulent flows, velocity and temperature profiles vary significantly near the channel wall and a nonuniform grid spacing must be employed to maintain a manageable number of grid points. The nodal positions were assigned according to the following expression [22]

$$\eta = \frac{1}{V_t}(e^{\xi} - 1); \quad \xi = \ln(\eta V_t + 1) \tag{31}$$

where $V_t\ (= 4Re_t)$ is a scaling factor whose purpose is to place more points in the vicinity of the wall. The constant utilized in V_t was selected after some numerical experiments were performed to establish the influence of nodal positions on the temperature distributions. The distance ξ_c as measured from the wall to the channel center where $\eta = 1$ in equation (31) is subdivided into $M-1$ equally spaced nodes. Equation (31) then yields a variable grid spacing for values of η with sufficient number of points near the channel wall. For the results presented here, $M = 51$ was found to provide accurate results within reasonable computational times.

RESULTS AND DISCUSSION

Parameter values

Before results from the analysis are presented, it is informative to identify physically representative values of the dimensionless quantities which govern the solutions. Values for the dimensional parameters were selected as typical of those for a large scale MHD generator such as the U-25 channel [14]. For this channel, the mean velocity is approximately 900 m/s, centerline temperatures are near 2800 K, wall temperatures may range from 1000 to 1800 K depending on the wall cooling system, electrode materials, and presence of a molten slag layer, channel widths vary from 0.35 to 0.75 m, the magnetic field is near 2 Webers/m^2, and the gas has an average electrical conductivity of 10 Ω^{-1} m^{-1}. Utilizing these values as well as gas property data taken from Bunde [24], representative values for the dimensionless parameters are $Re_D = 3 \times 10^6$, $Ha = 200$, $Ec = 0.2$, and $N = 0.0001$ to 0.01 with $\tau_0 = 0.1$ to 10. Definitive values for τ_0 are unavailable; however, Wilson and Haji-Sheikh [5] quoted an absorption coefficient of 0.0001 m^{-1} for a small scale MHD channel, and Smith and Paul [12] reported optical thicknesses ranging from 1 to 10 for a gas composition similar to that in the U-25 channel. In selection of values for the governing parameters, cognizance was made of these approximate but physically meaningful values of the parameters.

Transparent gas

Representative velocity and temperature profiles for a transparent gas displayed in Figs. 2 and 3, respectively, are intended to illustrate the turbulent characteristics and behavior of the results. Profiles are shown for OHD and MHD flows with hydraulic

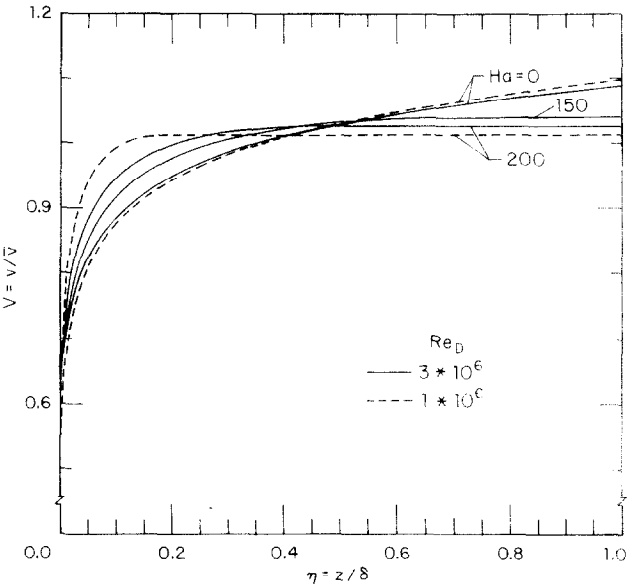

FIG. 2. Velocity profiles.

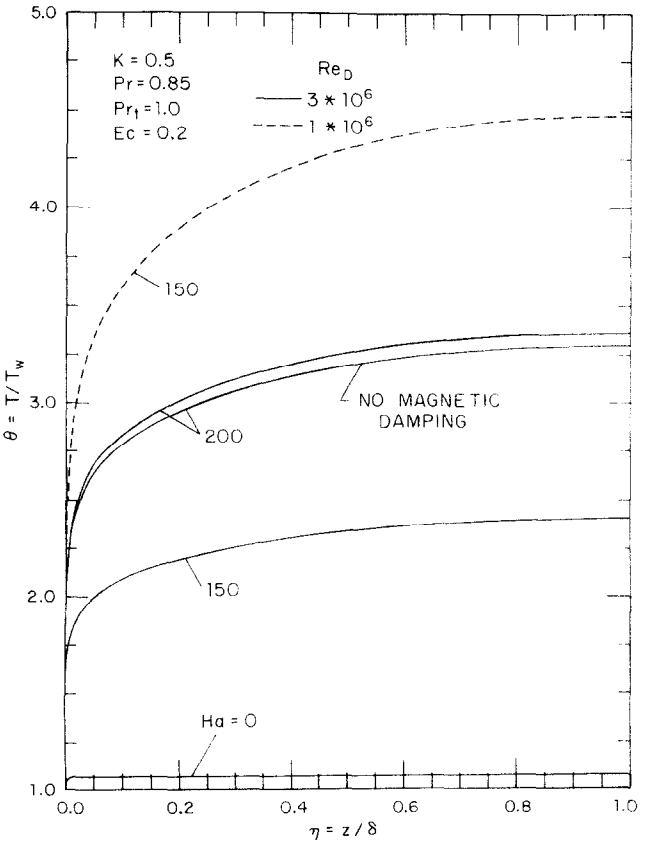

FIG. 3. Temperature profiles for a transparent gas.

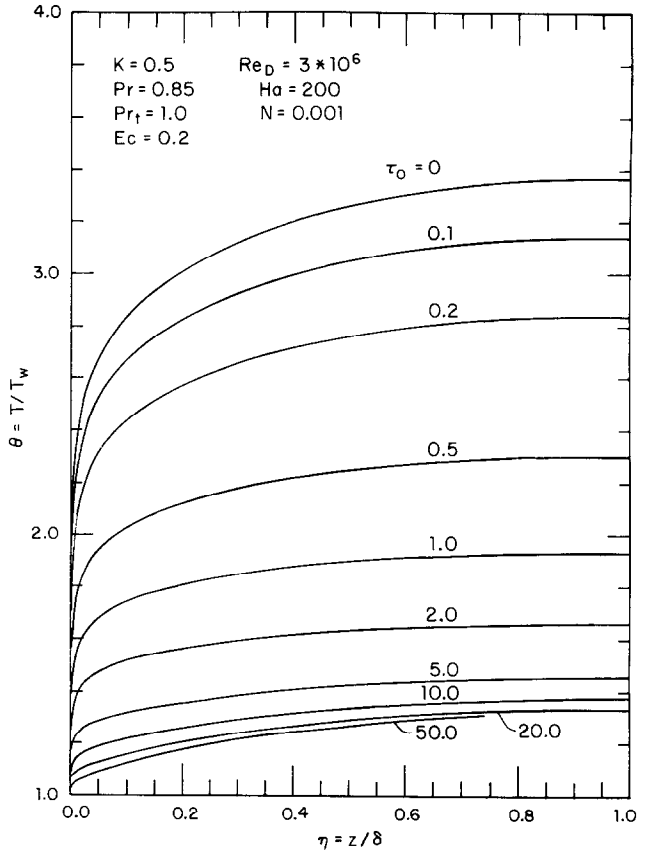

FIG. 4. Temperature profiles as a function of optical thickness.

Reynolds numbers of 1×10^6 and 3×10^6 and Hartmann numbers of zero for the OHD results and 150 and 200 for the MHD flows. The OHD velocity profiles are based on the universal turbulent profiles with the coefficient of friction evaluated from the Filonenko expression [25]. The OHD velocity profiles exhibit smaller gradients near the wall and lower mean velocities than the MHD velocity profile for the same centerline velocities. As the Hartmann increases the profiles become more uniform with higher gradients near the wall. For the OHD velocity profiles, higher Reynolds numbers produce flatter profiles and steeper velocity gradients near the wall. However, for the MHD velocity profiles, higher Reynolds numbers produce the opposite effect as displayed by results for $Ha = 200$. As presently modeled, the magnetic damping function in the turbulent viscosity expression does not influence the velocity profiles. The OHD temperature profiles in Fig. 3 are the result of viscous dissipation and exhibit values near 1.07 for the two Reynolds numbers. The inclusion of the Joulean heating term in the energy equation is seen to produce significantly higher gas temperatures for MHD flows than for the OHD case. Values of the Hartmann number of 150 and 200 produce, respectively, centerline temperatures of 2.4 and 3.4 for $Re_D = 3 \times 10^6$. Decreasing the Reynolds number results in higher gas temperatures since the transport of energy due to Joulean heating by the turbulent mechanism is reduced. Results are also presented in Fig. 3 for a magnetic damping function of unity in equation (8), that is the OHD form. The damping function for $Re_D = 3 \times 10^6$ and $Ha = 200$ has a value of 0.96. The inclusion of the damping function produces higher gas temperatures since the turbulent viscosity is reduced resulting in less energy being transported to the wall. In comparison with temperatures evaluated for Hartmann MHD flow where laminar flow is assumed [5, 12, 13], the present temperature profiles are for significantly higher Hartmann numbers. Thus, by including turbulent transport in the energy equation, higher Hartmann numbers are possible with physically reasonable temperature profiles.

Radiating gas

Representative temperature profiles for a radiatively participating gas are displayed in Fig. 4 for Reynolds and Hartmann numbers of 3×10^6 and 200, respectively, and $N = 0.001$. Results are presented for channel optical thicknesses ranging from zero corresponding to a transparent gas to 50. Values for the other governing parameters are provided in the figure.

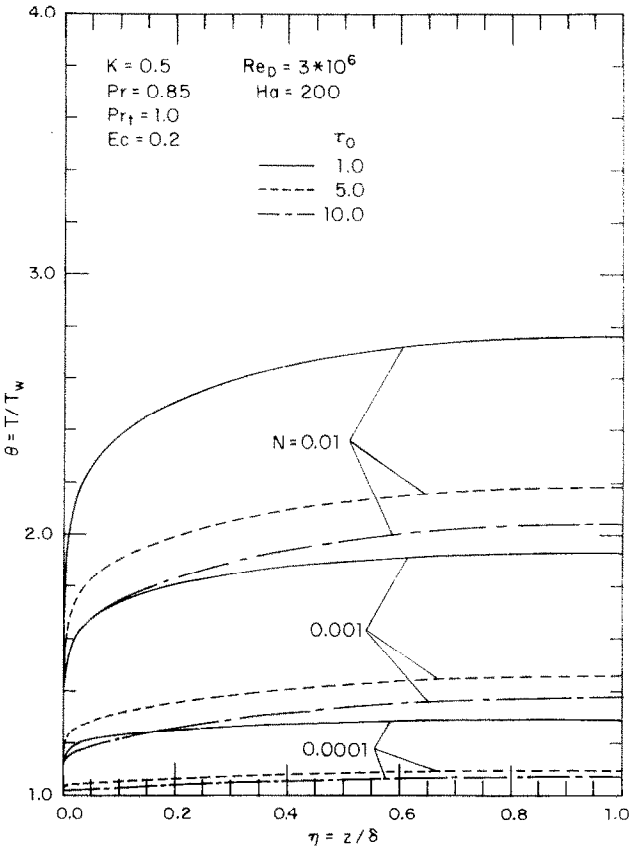

FIG. 5. Effect of conduction–radiation parameter.

As the optical thickness increases from 0 to 10.0, significant decreases in gas temperatures are observed. For optical thicknesses less than about 0.1, the results are adequately described by those when the gas is assumed to be optically thin [16]. For optical thicknesses greater than 10.0, gas temperatures continue to decrease and become nearly insensitive to optical thickness particularly near the channel centerline. At very large optical thicknesses corresponding to an optically thick gas, the product of the divergence of the radiative heat flux and square of the channel optical thickness is independent of optical thickness [16]. Thus, the gas temperatures as observed by equation (3) become independent of the optical thickness. For the anticipated optical thickness range of 1 to 10, centerline gas temperatures vary from approximately 1.4 to 2.0 higher than the wall temperatures.

Effects of the conduction–radiation parameter on gas temperature profiles are illustrated in Fig. 5 where results are shown for values of the parameter equal to 0.0001, 0.001 and 0.01 with optical thicknesses of 1.0, 5.0 and 10.0. As the conduction–radiation parameter decreases, the radiative term in equation (3) becomes more significant with a resultant decrease in gas temperatures. The optically thick limit where gas temperatures are independent of optical thickness is attained at smaller values of the optical thickness for the lower values of the conduction–radiation parameter.

The influence of the Reynolds and Hartmann numbers is demonstrated in Fig. 6 where gas temperature profiles are presented for $N = 0.001$, $\tau_0 = 5.0$, and several values the Reynolds and Hartmann numbers. As expected, higher Hartmann numbers produce higher gas temperatures and higher Reynolds numbers yield lower profiles as a result of the increase turbulent transport. Gas temperatures are observed to be more sensitive to the higher values of the Reynolds number.

Nusselt numbers

In Table 1, results are tabulated for the bulk temperature, as well as convective, radiative, and total Nusselt numbers for various values of the governing parameters. The table is organized into four groups corresponding to temperature profiles presented in Figs. 3–6. The first group of results is for a transparent gas. The OHD flow produces a convective Nusselt number of 7310 for $Re_D = 3 \times 10^6$. Experimental measurements for OHD turbulent flow [26] yield a Stanton number correlation from which a Nusselt

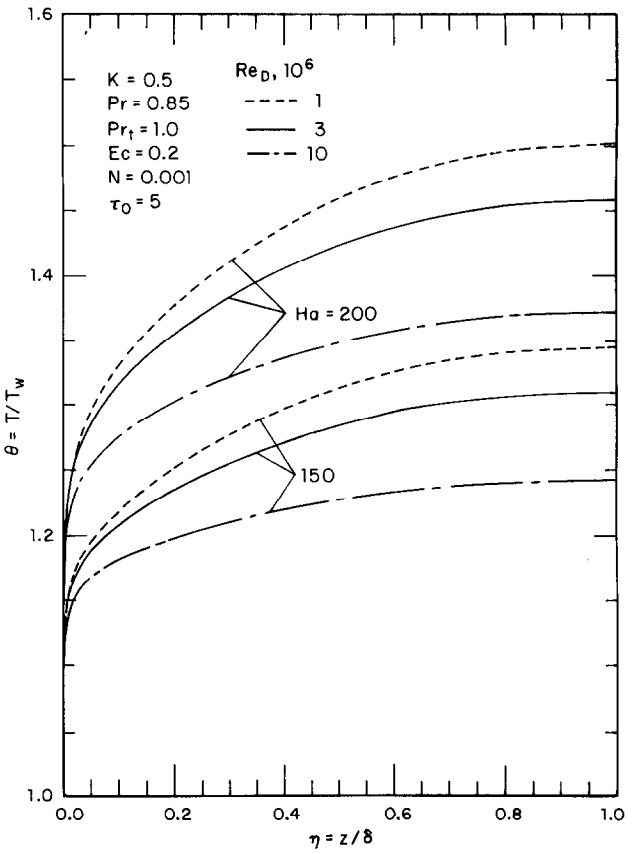

FIG. 6. Effect of Reynolds and Hartmann numbers.

Table 1. Bulk temperatures and Nusselt numbers*

Re_D, 10^6	Ha	N	τ_0	θ_b	Nu_c, 10^4	Nu_r, 10^4	Nu, 10^4
3	0	0	0	1.07	0.731	0.0	0.731
1	150			4.17	0.139	0.0	0.139
3	150			2.30	0.395	0.0	0.395
3	200			3.18	0.371	0.0	0.371
3	200	0.001	0.1	2.98	0.378	0.066	0.445
			0.2	2.70	0.391	0.183	0.574
			0.5	2.21	0.427	0.521	0.948
			1.0	1.87	0.475	0.978	1.45
			2.0	1.61	0.540	1.66	2.20
			5.0	1.41	0.626	2.86	3.49
			10.0	1.32	0.667	3.87	4.54
			20.0	1.27	0.680	4.76	5.44
			50.0	1.24	0.654	5.29	5.94
3	200	0.01	1.0	2.63	0.396	0.218	0.614
			5.0	2.09	0.434	0.652	1.09
			10.0	1.94	0.438	0.881	1.32
		0.0001	1.0	1.27	0.826	4.54	5.37
			5.0	1.08	1.98	17.4	19.4
			10.0	1.06	2.54	24.0	26.5
1	150	0.001	5.0	1.30	0.373	2.44	2.81
3				1.27	0.732	2.40	3.13
10				1.22	2.13	2.36	4.49
1	200			1.44	0.289	2.92	3.21
3				1.41	0.626	2.86	3.49
10				1.34	1.70	2.72	4.43

* Results are for $K = 0.5$, $Pr = 0.85$, $Pr_t = 1.0$, $Ec = 0.2$.

number of 7100 is calculated for $Re_D = 3 \times 10^6$. Thus, the results presented here for OHD appear reasonable. As the Hartmann number is increased, the convective Nusselt number decreases since the increase in temperature gradient at the wall is offset by a more rapid increase in bulk temperature. Results in the second group for a radiating gas illustrate that as the channel optical thickness increases, the convective Nusselt number increases and then decreases for optical thicknesses greater than about 20.0. The radiative Nusselt number continues to increase with optical thickness and shows a tendency of becoming independent of optical thickness which is characteristic of an optically thick gas. The radiative Nusselt number is the significant contributor to the total Nusselt number for optical thicknesses greater than 5.0. As the conduction—radiation parameter is increased, the Nusselt numbers presented in the third group exhibit large increases with optical thickness particularly for values of this parameter less than 0.001. Convective Nusselt numbers for values of the conduction-radiation parameter less than 0.01 are nearly independent of the optical thickness. The Nusselt numbers for $N = 0.001$ exhibit rather significant increases as the optical thickness is varied from 0.5 to 10.0 even though the corresponding gas temperature profiles in Fig. 5 and bulk temperatures in Table 1 change only slightly. The fourth group of results shows that as the Hartmann number is increased from 150 to 200, convective Nusselt numbers decrease but radiative Nusselt numbers increase, and total Nusselt numbers increase except for $Re_D = 10^7$ where a small decrease is found. Increasing the Reynolds number from 10^6 to 10^7 produces significant increases in the convective Nusselt number, and small decreases in the radiative Nusselt number. These trends are consistent with the temperature levels and gradients in Fig. 6.

CONCLUSIONS

Analyses and results have been presented to examine the influence of gas radiation on temperature profiles for fully developed turbulent MHD flow. Representative models for turbulent gas velocity profiles as a function of the Reynolds and Hartmann numbers, turbulent viscosity with a magnetic damping function, current density, and radiative transfer for an absorbing and emitting gas with constant absorption coefficient were introduced. Analyses were also presented for gas bulk temperature as well as convective, radiative, and total Nusselt numbers. The results illustrated that gas radiation lowers significantly gas temperatures. Higher Hartmann numbers yield higher gas temperatures but higher Reynolds numbers produce lower temperatures as a result of the increased turbulent transport. The convective Nusselt number remains nearly constant as the optical thickness increased. At intermediate to large values of optical thickness, the radiative Nusselt number dominates the convective Nusselt number and exhibits a strong dependency on optical thickness.

REFERENCES

1. A. W. Postlethwaite and M. M. Sluyter, MHD heat transfer problems—an overview, *Mech. Engng* 32–39, March (1978).
2. R. Viskanta, Effect of transverse magnetic field on heat transfer to an electrically conducting and thermally radiating fluid flowing in a parallel-plate channel, *Z. Angew. Math. Phys.* **14,** 353–368 (1963).
3. R. Viskanta, Some considerations of radiation in magnetohydrodynamic Couette flow, *Z. Angew. Math. Phys.* **15,** 227–236 (1964).
4. K. R. Cramer and S. Pai, *Magnetofluid Dynamics for Engineers and Applied Physicists.* McGraw-Hill, New York (1973).
5. D. R. Wilson and A. Haji-Sheikh, Effect of radiative cooling on the temperature distribution in MHD channel flows, *J. Heat Transfer* **97,** 151–152 (1975).
6. P. S. Gupta and A. S. Gupta, Radiation effect on hydromagnetic convection in a vertical channel, *Int. J. Heat Mass Transfer* **17,** 1437–1442 (1974).
7. N. Datta and R. N. Janta, Effect of wall conductances on hydromagnetic convection of a radiating gas in a vertical channel, *Int. J. Heat Mass Transfer* **19,** 1015–1019 (1976).
8. J. B. Helliwell, Effects of thermal radiation in magnetohydrodynamic channel flow, *J. Engng Math* **7,** 11–17 (1973).
9. J. B. Helliwell, Effects of thermal conductivity in radiative magnetohydrodynamic channel flow, *J. Engng Math.* **7,** 347–350 (1973).
10. J. B. Helliwell and M. F. Mosa, Radiative heat transfer in horizontal magnetohydrodynamic channel flow with buoyancy effects and an axial temperature gradient, *Int. J. Heat Mass Transfer* **22,** 657–667 (1979).
11. W. G. Vincenti and C. H. Kruger, *Introduction to Physical Gas Dynamics.* John Wiley, New York (1965).
12. T. F. Smith and P. H. Paul, Radiative transfer in Hartmann MHD Flow, *J. Heat Transfer* **101,** 502–506 (1979).
13. G. W. Sutton and A. Sherman, *Engineering Magnetohydrodynamics.* McGraw-Hill, New York (1965).
14. T. R. Brogan, A. M. Aframe and J. Hill, Preliminary design of a magnetohydrodynamic channel for the USSR U-25 facility, MEPPSCO Inc. (1974).
15. H. McDonald and J. P. Kreskovsky, Effect of free stream turbulence on the turbulent boundary layer, *Int. J. Heat Mass Transfer* **17,** 705–716 (1974).
16. E. M. Sparrow and R. D. Cess, *Radiation Heat Transfer—Augmented Edition.* McGraw-Hill, New York (1978).
17. C. H. Kruger and O. K. Sonju, On the turbulent magnetohydrodynamic boundary layer, *Proceedings of the* 1964 *Heat Transfer & Fluid Mechanics Institute,* pp. 147–159. Stanford University Press, Stanford, CA (1964).
18. L. P. Harris, *Hydromagnetic Channel Flows,* MIT Technology Press and John Wiley (1960).
19. E. R. Van Driest, On turbulent flow near a wall, *J. Aero. Sci.* **23,** 1007–1011 (1956).
20. J. Mei and W. Squire, A simple eddy viscosity model for turbulent pipe and channel flow, *AIAA Jl* **10,** 350–352 (1972).
21. W. A. Fiveland, An analytical study of laminar and turbulent magnetofluid dynamic boundary layer flow with heat transfer, Ph.D. Thesis, University of Akron, Ohio (1978).
22. D. K. Edwards and A. Balakrishnan, Nongray radiative transfer in a turbulent gas layer, *Int. J. Heat Mass Transfer* **16,** 1003–1015 (1973).

23. J. O. Mingle, An improved solution of the Q-problem for radiative equilibrium, *Letters Heat Mass Transfer* **2**, 135–140 (1975).
24. R. Bunde, H. Muntenbruch, J. Raeder, R. Volk and G. Zankl, *MHD Power Generation*. Springer, Berlin (1975).
25. B. V. Karlekar and R. M. Desmond, *Engineering Heat Transfer*. West (1977).
26. A. Gador and J. F. Louis, Measurement of radiative and convective heat transfer rates and skin friction in an MHD flow, AIAA, Paper No. 79–1537 (1979).

ECOULEMENT TURBULENT MHD D'UN GAZ RAYONNANT

Résumé—Les hautes températures et les produits gazeux de la combustion des hydrocarbures dans des générateurs MHD de grande taille nécessitent le développement de modèles précis pour la prédiction des profils de température des gaz et des flux thermiques pariétaux. Aux températures élevées et pour les grandes tailles, le transfert thermique par rayonnement dans les gaz de combustion peut être le mécanisme principal de transfert d'énergie. On présente des résultats sur les profils de température de gaz pour l'écoulement MHD turbulent développé d'un gaz gris qui rayonne entre deux plans parallèles infinis avec un champ magnétique appliqué perpendiculairement aux plans. On port attention aux profils de température et au nombre de Nusselt pour différentes valeurs de nombres de Hartmann et de Reynolds, différentes épaisseurs optiques de gaz et pour le paramètre de couplage conduction-rayonnement.

TURBULENTE MAGNETO-HYDRODYNAMISCHE STRÖMUNG EINES STRAHLENDEN GASES

Zusammenfassung—Die hohen Temperaturen und die gasförmigen Produkte bei der Verbrennung von kohlenwasserstoffhaltigen Brennstoffen in vorgeschlagenen großen magnetohydrodynamischen Generatoranlagen erfordern die Entwicklung genauer Modelle zur Berechnung der Temperaturprofile im Gas und der Wärmestromdichten an der Wand. Bei den hohen Temperaturen und großen Abmessungen wird der Strahlungswärmeaustausch in den Verbrennungsgasen ein bedeutender Wärmeübertragungsmechanismus sein. Es werden Ergebnisse für Temperaturprofile im Gas dargestellt für den Fall der voll ausgebildeten turbulenten magnetohydrodynamischen Strömung eines grau strahlenden Gases zwischen zwei unendlichen parallelen Platten. Senkrecht zu den Platten wirkt das magnetische Feld. Besonderes Gewicht wird auf die Untersuchung von Temperaturprofilen und Nusselt-Zahlen für verschiedene Werte der Hartmann- und Reynolds-Zahl, der optischen Dicke des Gases sowie des Verhältnisses zwischen Wärmeleitung und Strahlung gelegt.

ТУРБУЛЕНТНОЕ МАГНИТОГИДРОДИНАМИЧЕСКОЕ ТЕЧЕНИЕ ИЗЛУЧАЮЩЕГО ГАЗА

Аннотация — Высокие температуры и газообразные продукты сгорания углеводородных топлив в крупных магнитогидродинамических генераторах потребовали разработки точных моделей для расчета профилей температуры газа и тепловых нагрузок на стенке. При высоких температурах и больших размерах установок лучистый теплоперенос в газообразных продуктах сгорания может быть важным механизмом переноса энергии. Представлены результаты по определению профилей температуры газа при полностью развитом турбулентном магнитогидродинамическом течении излучающего серого газа между бесконечными параллельными пластинами, перпендикулярно к которым приложено магнитное поле. Особое внимание обращено на профили температуры, число Нуссельта при различных значениях чисел Гартмана и Рейнольдса, оптической толщины газа и параметра, описывающего соотношение между теплопроводностью и излучением.